SPANDIDOS PUBLICATIONS

ONCOLOGY REPORTS 41: 2103-2116, 2019

MicroRNA-92a promotes cell proliferation, migration and survival by directly targeting the tumor suppressor gene *NF2* in colorectal and lung cancer cells

KRIZELLE MAE M. ALCANTARA and REYNALDO L. GARCIA

National Institute of Molecular Biology and Biotechnology, University of the Philippines, Diliman, Quezon City 1101, Philippines

Received October 5, 2018; Accepted February 5, 2019

DOI: 10.3892/or.2019.7020

Abstract. Inactivation of the tumor suppressor protein Merlin leads to the development of benign nervous system tumors in neurofibromatosis type 2 (NF2). Documented causes of Merlin inactivation include deleterious mutations in the encoding neurofibromin 2 gene (*NF2*) and aberrant Merlin phosphorylation leading to proteasomal degradation. Rare somatic *NF2* mutations have also been detected in common human malignancies not associated with NF2, including colorectal and lung cancer. Furthermore, tumors without *NF2* mutations and with unaltered *NF2* transcript levels, but with low Merlin expression, have been reported. The present study demonstrated that *NF2* is also regulated by microRNAs (miRNAs) through direct interaction with evolutionarily conserved miRNA response elements (MREs) within its 3'-untranslated region (3'UTR). Dual-Luciferase assays in human colorectal carcinoma (HCT116) and lung adenocarcinoma (A549) cells revealed downregulation of *NF2* by miR-92a-3p via its wild-type 3'UTR, but not *NF2*-3'UTR with mutated miR-92a-3p MRE. HCT116 cells overexpressing miR-92a-3p exhibited significant downregulation of endogenous *NF2* mRNA and protein levels, which was rescued by co-transfection of a target protector oligonucleotide specific for the miR-92a-3p binding site within *NF2*-3'UTR. miR-92a-3p overexpression in HCT116 and A549 cells promoted migration, proliferation and resistance to apoptosis, as well as altered F-actin organization compared with controls. Knockdown of *NF2* by siRNA phenocopied the oncogenic effects of miR-92a overexpression on HCT116 and A549 cells. Collectively, the findings of the present study provide functional proof of the unappreciated role of miRNAs in *NF2* regulation and tumor progression, leading to enhanced oncogenicity.

Correspondence to: Dr Reynaldo L. Garcia, National Institute of Molecular Biology and Biotechnology, University of the Philippines, 3/F NIMBB Building, National Science Complex, Diliman, Quezon City 1101, Philippines
E-mail: reygarcia@mbb.upd.edu.ph

Abbreviations: NF2, neurofibromin 2; NF2, neurofibromatosis type 2; miRNA, microRNA; MRE, microRNA response element; 3'UTR, 3'-untranslated region; siRNA, small interfering RNA; EMT, epithelial-mesenchymal transition

Key words: neurofibromin 2 gene, neurofibromatosis type 2, microRNA, colorectal cancer, lung cancer, tumor suppressor, proliferation, migration, apoptosis, cytoskeletal organization

Introduction

The tumorigenic consequences of neurofibromin 2 gene (*NF2*) inactivation and the resulting downregulation of its encoded protein, Merlin, were first elucidated in the hereditary cancer-predisposing syndrome referred to as neurofibromatosis type 2 (NF2; OMIM 101000) (1). Classical NF2 is characterized by benign tumors of the nervous system, with the hallmark symptoms including bilateral vestibular schwannomas, meningiomas, and ependymomas (2). Merlin regulates contact-dependent inhibition of growth via signal transduction pathways controlling cell proliferation and survival (2,3). Merlin also acts as a molecular scaffold between transmembrane receptors and the cortical actin cytoskeleton, thus, regulating functions such as cell morphogenesis, adhesion and migration (3).

Studies investigating Merlin regulation and tumorigenesis mainly focus on mutational events within the coding region of *NF2* leading to loss of functional protein expression (4). *De novo* mutations in *NF2* have been reported in 50-60% of NF2 cases (2,5). Notably, rare somatic mutations in *NF2* have also been detected in common human malignancies not associated with NF2, including but not limited to mesotheliomas, melanomas, colorectal, lung, breast, hepatic, prostate and thyroid carcinomas (2,6,7).

Despite the low prevalence of *NF2* mutations in cancer (6), there is mounting evidence that inactivation of Merlin may be involved in cancer development and progression. Čačev *et al* reported that *NF2* mRNA and protein expression were significantly lower in poorly differentiated colorectal carcinoma compared with well-differentiated tumors (8). In a breast cancer cohort, 75% (56/75) of tumors without *NF2* mutations were found to have unaltered *NF2* transcript levels but markedly low Merlin expression. This was correlated with

increased metastatic potential, which was reversed by rescuing Merlin expression (9). Those studies indicated that there are mechanisms other than deleterious mutations, proteasomal degradation or *NF2* promoter methylation, all of which have not been consistently observed across malignancies (4,8-10), that may be involved in Merlin inactivation leading to tumorigenesis.

One possible mechanism is post-transcriptional regulation of *NF2* expression by microRNAs (miRNAs). Endogenously expressed miRNAs have been shown to play key roles in cancer by regulating oncogenes and tumor suppressor genes through miRNA response elements (MREs) within their 3' untranslated region (3'UTR) (11). For Merlin, however, there is paucity of information on whether its expression and tumor suppressor function are endogenously regulated by specific miRNA species (4).

To elucidate the role of miRNAs in regulating *NF2*, the 3'UTR sequence of wild-type *NF2* was analyzed *in silico*. Among the candidate miRNAs identified, hsa-miR-92a-3p was found to downregulate endogenous *NF2* mRNA and protein expression in HCT116 colorectal cancer cells. Overexpression of miR-92a-3p in HCT116 and A549 lung adenocarcinoma cells disrupted contact-mediated inhibition of proliferation and enhanced cell migration, proliferation and survival. Changes in F-actin organization were also observed in miR-92a-3p-overexpressing A549 cells. These functional readouts were phenocopied by siRNA knockdown of *NF2*. Collectively, these results indicated that miR-92a-3p can post-transcriptionally regulate *NF2* and contribute, at least partially, to the negative regulation of the tumour-suppressive functions of Merlin by targeting the *NF2*-3'UTR, leading to enhanced oncogenicity.

Materials and methods

Cell culture. The human colorectal carcinoma cell line HCT116 and the human lung adenocarcinoma cell line A549 were sourced from the American Type Culture Collection (ATCC; Manassas, VA, USA). HCT116 cells were cultured in RPMI-1640 medium supplemented with 10% fetal bovine serum (FBS) (Gibco; Thermo Fisher Scientific, Inc., Waltham, MA, USA), 50 U/ml penicillin/streptomycin and 2.0 g/l sodium bicarbonate. A549 cells were cultured in Dulbecco's modified Eagle's medium (DMEM) (Gibco; Thermo Fisher Scientific, Inc.) supplemented with 10% FBS, 50 U/ml penicillin/streptomycin and 3.7 g/l sodium bicarbonate. All the cells were maintained in a 37˚C humidified incubator with 5% CO_2.

Cell transient transfection. HCT116 cells were seeded for assays in 12-well plates at 300,000 cells/well and in 96-well plates at 10,000 cells/well. A549 cells were seeded for assays in 12-well plates at 200,000 cells/well and in 96-well plates at 5,000 cells/well. All transfection experiments were performed using Lipofectamine® 2000 (Invitrogen; Thermo Fisher Scientific, Inc.) according to the manufacturer's instructions. The amount of plasmid and volume of Lipofectamine 2000 were optimized to achieve 70-80% transfection efficiency for all functional and molecular characterizations.

Antibodies and plasmid constructs. The rabbit polyclonal anti-*NF2* (dilution 1:1,200; cat. no. PA5-35316) and mouse monoclonal anti-N-cadherin (dilution 1:1,500; cat. no. MA5-15633) antibodies were obtained from Invitrogen (Thermo Fisher Scientific, Inc.). The rabbit polyclonal anti-E-cadherin (dilution 1:7,500; cat. no. 07-697) and mouse monoclonal anti-GAPDH (dilution 1:1,500; cat. no. CB1001) antibodies were obtained from EMD Millipore (Burlington, MA, USA). The rabbit polyclonal anti-vimentin antibody (dilution 1:700; cat. no. SAB4503083) was purchased from Sigma-Aldrich; Merck KGaA (Darmstadt, Germany). The goat anti-mouse IgG (H+L) (dilution 1:10,000; cat. no. 31430) and goat anti-rabbit IgG (dilution 1:5,000 cat. no. 31460) secondary antibodies conjugated with horseradish peroxidase were obtained from Invitrogen (Thermo Fisher Scientific, Inc.).

The 3'UTR of human *NF2* isoform I (NM_000268.3) and the pre-miR-92a-1 gene (NR_029508.1) were amplified in a polymerase chain reaction (PCR) reaction mixture containing a final concentration of 1X PCR buffer (Titanium® Taq PCR buffer; Clontech Laboratories, Inc., Mountain View, CA, USA), 0.125 μM of each deoxynucleoside triphosphate (dNTPs) (Promega Corporation, Madison, WI, USA), 2 μM each of the forward and reverse primers, 1X Taq polymerase (Titanium® Taq polymerase; Clontech Laboratories, Inc.) and wild-type human genomic DNA template available in the Disease Molecular Biology and Epigenetics Laboratory of the National Institute of Molecular Biology and Biotechnology (DMBEL-NIMBB). The cycling conditions were as follows: Initial denaturation at 94˚C for 5 min, followed by 25-30 cycles of denaturation at 94˚C for 30 sec, annealing at 55˚C for 30 sec, and extension at 72˚C for 30 sec, with a final extension step at 72˚C for 10 min.

The wild-type *NF2*-3'UTR fragment was cloned into the pmirGLO Dual-Luciferase miRNA target expression vector (Promega Corporation), downstream of the firefly luciferase gene. A mutant version of the *NF2*-3'UTR was generated by site-directed mutagenesis of the wild-type *NF2*-3'UTR in pmirGLO, in which a CA>GT substitution within the miR-92a-3p seed sequence-binding site (5'-GTG<u>CA</u>AT-3') was introduced through overlap extension PCR. The pre-miR-92a-1 amplicon was amplified using primers targeting the flanking genomic DNA template 173 bp upstream and 176 bp downstream of the pre-miRNA sequence (Chr. 13q31.3; NC_000013.11 region: 91351141.91351567) and was cloned into the mammalian microRNA expression vector pmR-ZsGreen1 (Clontech Laboratories, Inc.). Mutation of the shared MRE of the miR-92a family resulted in the removal of its members (miR-92a, miR-92b, miR-25, miR-32, miR-363 and miR-367) from the list of miRNAs predicted to bind to the mutant 792-bp fragment of *NF2*-3'UTR, as analyzed using the MirTarget custom prediction function of miRDB (12) (Table I). No new unintended miRNA binding sites were introduced to the mutant *NF2*-3'UTR. The primer sequences are listed in Table II.

QuantiGene evaluation of miRNA expression in HCT116 and A549 cells. For direct quantification of mature miR-92a-3p in control and transfected HCT116 and A549 cells, QuantiGene miRNA Assay (Affymetrix; Thermo Fisher Scientific, Inc.) was used. QuantiGene Singleplex miRNA probes were obtained from the pre-designed probes offered by eBioscience (Thermo Fisher Scientific, Inc.). The custom probe for

Table I. List of MirTarget predicted miRNAs that bind to the wild-type and miR-92a-MRE mutant *NF2*-3'UTR.

Target rank	Target score	miRNA name	Seed locations
NF2-3'UTR-wt and mut-92a			
1	83	hsa-miR-4486	310,383,501
2	78	hsa-miR-4447	408
3	68	hsa-miR-1275	407
4	66	hsa-miR-6780b-p	755
5	66	hsa-miR-4725-3p	755
6	66	hsa-miR-4271	755
7	61	hsa-miR-216b-5p	162
8	59	hsa-miR-4684-5	160
9	58	hsa-miR-7106-3p	60,493
10	53	hsa-miR-4731-5p	101
11	53	hsa-miR-7-5p	222,753
12	51	hsa-miR-7152-3p	33
NF2-3'UTR-wt only			
13	50	hsa-miR-92a-3p	134
14	50	hsa-miR-92b-3p	134
15	50	hsa-miR-367-3p	134
16	50	hsa-miR-363-3p	134
17	50	hsa-miR-32-5p	134
18	50	hsa-miR-25-3p	134

Mutation of the MRE resulted in the removal of miR-92a members (miR-92a, miR-92b, miR-25, miR-32, miR-363 and miR-367) from the list of miRNAs predicted to bind to the mutant 792-bp fragment of NF2-3'UTR. *NF2*, neurofibromin 2; UTR, untranslated region; MRE, microRNA response element.

Table II. Primers used for construct generation, site-directed mutagenesis and qPCR.

Designation	Sequence (5' to 3')	RE site
NF2-3'UTR-F	CACTACGCTAGCTGCCACTTCTCCTGCTAC	*Nhe*I
NF2-3'UTR-R	ACTTATGTCGACCAGGAAGGAGCGTCTATG	*Sal*I
miR-92a-F	CACTACCTCGAGGTAGAACTCCAGCTTCGG	*Xho*I
miR-92a-R	ACTTGCGGATCCCAAATCTGACACGCAACC	*Bam*HI
NF2-miR-92a-mutF	GCCCCTCTTATGTGGTATTGCCTTGAACTA	None
NF2-miR-92a-mutR	TAGTTCAAGGCAATACCACATAAGAGGGGC	None
NF2-qPCR-F	TGCGAGATGAAGTGGAAAGG	None
NF2-qPCR-R	GCCAAGAAGTGAAAGGTGAC	None
GAPDH-qPCR-F	GACCTGACCTGCCGTCTAGAAAAAC	None
GAPDH-qPCR-R	CCATGAGGTCCACCACCCTGTTG	None

NF2, neurofibromin 2; UTR, untranslated region; F, forward; R, reverse; mut, mutant; RE, restriction enzyme.

miR-92a-3p (5'-UAUUGCACUUGUCCCGGCCUGU-3') had previously been functionally validated for sensitivity and specificity for mature miR-92a-3p in human samples and had also been evaluated for cross-reactivity towards closely related miRNA family members. Cultured HCT116 and A549 cells were subjected to the assay according to the manufacturer's instructions. The luminescent signal generated was measured using a plate-reading luminometer (FLUOstar Omega microplate reader; BMG Labtech, Cary, NC, USA). Triplicates of cell lysates per setup of untransfected cells (maintained in media supplemented with 10 and 0.5% serum) and pmR-ZsGreen1-miR-92a-transfected cells were subjected to the assay. Average signals-background of samples were interpolated in a standard curve generated using serial dilutions of

synthetic miR-92a-3p-positive control to calculate the average mature miR-92a-3p expression copy number in each experimental setup.

Dual-luciferase assay. For the endogenous dual-Luciferase assays, cells were seeded in 96-well plates and transfected with 200 ng of empty pmirGLO vector (Promega Corporation) or pmirGLO-*NF2*-3'UTR-wild-type. For the miRNA co-transfection Dual-Luciferase assays, cells were co-transfected with 20 ng of empty pmirGLO vector, pmirGLO-*NF2*-3'UTR-wild-type, or pmirGLO-*NF2*-3'UTR-mut92a along with 200 ng of empty pmR-ZsGreen1 vector (Clontech Laboratories, Inc.) or pmR-ZsGreen1-miR-92a construct. Luciferase activity was determined at 48 h post-transfection using the Dual-Luciferase® Reporter Assay system (Promega Corporation) and the GloMax 20/20 luminometer (Promega Corporation) following the manufacturer's instructions. Data are expressed as mean values of normalized firefly relative luciferase units (RLUs) per setup. Raw firefly RLUs were first normalized against internal control *Renilla* luciferase RLUs per well before normalizing against values obtained for the empty vector control setup.

Target protector experiments. HCT116 cells were co-transfected with pmR-ZsGreen1-miR-92a and a target protector oligonucleotide specific to the conserved MRE of hsa-miR-92a-3p within the 3'UTR of the *NF2* gene. The oligonucleotide was designed using Qiagen's miRNA target protector design tool (https://www.qiagen.com/ph/shop/genes-and-pathways/custom-products/custom-assay-products/custom-mirna-products/#target-protector) using the RefSeq ID of *NF2* transcript variant 1 (NM_000268) as a reference template. An effective concentration of 100 nM miR-92a target protector co-transfected with pmR-ZsGreen1-miR-92a (final concentration, 2 ng/μl) was determined through preliminary transfection optimization experiments. The efficiency of miRNA inhibition by the target protector was measured using reverse transcription-quantitative PCR (RT-qPCR) or western blotting of lysates from transfected cells vs. control setups.

NF2 siRNA knockdown experiments. To facilitate specific knockdown of the *NF2* gene and directly observe its functional consequences, cells were transfected with a 21-nt siRNA oligonucleotide (Qiagen Sciences, Inc., Germantown, MD, USA; Hs_NF2_7; 5'-CACCGTGAGGATCGTCACCAT-3') directed against all known transcript variants of human *NF2*. The effective concentration of Hs_NF2_7 siRNA oligo was determined to be 5 nM using preliminary transfection optimization experiments with Lipofectamine 2000 (Invitrogen; Thermo Fisher Scientific, Inc.). The efficiency of siRNA knockdown of *NF2* was assessed using RT-qPCR or western blotting of lysates from transfected cells vs. negative control setups.

RT-qPCR. HCT116 cells seeded in 12-well plates were transfected after 24 h with 2 μg of empty pmR-ZsGreen1 or pmR-ZsGreen1-miR92a construct. The cells were harvested at 48 h post-transfection and total RNA was extracted using TRIzol® reagent (Invitrogen; Thermo Fisher Scientific, Inc.). First-Strand cDNA was generated from 2 μg total RNA per setup using M-MLV Reverse Transcriptase (Promega Corporation) and oligo-dT primers, according to the manufacturer's protocol. The First-Strand cDNA samples were then used as templates for semi-RT-qPCR and RT-qPCR with SYBR® Select Master Mix (Invitrogen; Thermo Fisher Scientific, Inc.) using the relative quantitation method. For semi-RT-qPCR, densitometric analysis of the digitized band intensities on the agarose gels were performed using GelQuant.NET software (v1.8.2) provided by biochemlabsolutions.com. Quantified *NF2* gene expression in triplicate experiments was normalized against GAPDH gene expression. For RT-qPCR, total *NF2* mRNA was normalized against GAPDH mRNA measured per sample. Mean values of triplicates per setup were obtained, and the fold-change of *NF2* expression relative to the empty vector control was calculated. The primers used for RT-qPCR are summarized in Table II.

Western blotting. HCT116 cells were seeded and transfected in 12-well plates as described for RT-qPCR. Cells were harvested 48 h post-transfection and total protein was extracted using radioimmunoprecipitation lysis buffer [(150 mM NaCl, 0.5% sodium deoxycholate, 0.1% sodium dodecyl sulphate, 50 mM Tris (pH 8.0)] supplemented with protease inhibitors [1 mM phenylmethylsulfonyl fluoride (PMSF), 5 mM EDTA and 10 μM E64 (Roche Diagnostics GmbH, Mannheim, Germany)]. For polyacrylamide gel electrophoresis, 30 μg of total protein per setup quantified through the BCA method was loaded into 4-15% Mini-PROTEAN® TGX Stain-Free™ Protein Gels (Bio-Rad Laboratories, Inc., Hercules, CA, USA) and blotted onto polyvinylidene difluoride (PVDF) membranes. The membranes were blocked with 5% w/v whey protein in Tris-buffered saline with 0.1% v/v Tween-20 (TBST) for 1 h at room temperature, probed overnight with the primary antibodies aforementioned, washed with TBST, and incubated with the appropriate secondary antibodies for 1 h at room temperature. Signals were developed with enhanced chemiluminescence substrate and imaged using the ChemiDoc Touch Imaging System (Bio-Rad Laboratories, Inc., Hercules, CA, USA). Densitometric analysis of digitized band intensities was performed using GelQuant.NET software (v1.8.2) provided by biochemlabsolutions.com. Gene expression levels were normalized against GAPDH expression.

Wound healing assay. Cells in 12-well plates were transfected 24 h after seeding with 2 μg of empty pmR-ZsGreen1 or pmR-ZsGreen1-miR-92a construct. Upon reaching >90% confluence, a thin artificial wound was created on the cell monolayer using a sterile 200-μl pipette tip. Cells were washed once with 1X phosphate-buffered saline (PBS), and maintained in the appropriate media supplemented with 10 or 2% FBS. Wound closure was monitored every 12 h by capturing three fields of view per setup at a magnification of x40 using an Olympus IX71 inverted fluorescence microscope (Olympus Corp., Tokyo, Japan). Percent open wound area was analyzed using the TScratch software (13) and reported as the mean % open wound area per setup relative to % open wound area upon initial scratching (t=0 h).

Cell proliferation assay. Cells in 96-well plates were transfected 24 h after seeding with 200 ng of empty pmR-ZsGreen1

or pmR-ZsGreen1-miR-92a construct and maintained in the appropriate media supplemented with 10 or 2% FBS. The number of metabolically active cells per setup was measured at 48, 72 and 96 h post-transfection upon incubation with 10 μl of CellTiter 96® Aqueous One Solution Cell Proliferation Assay reagent (Promega Corporation) per well, until color development. Absorbance values at 460 nm of each setup were measured with a colorimetric plate reader (FLUOstar Omega microplate reader; BMG Labtech). Cell counts were calculated from a standard curve (number of cells vs. A_{460}) generated using serial dilutions of an untransfected cell suspension. Mean cell counts were calculated per setup for each time-point.

Caspase-3/7 assay. Cells were seeded in 96-well plates and transfected in triplicate, as described above. HCT116 cells were incubated in RPMI-1640 media supplemented with 10 or 2% FBS alone, or with 2.5 mM sodium butyrate for induction of apoptosis. A549 cells were incubated in DMEM supplemented with 10% FBS or without FBS. Caspase-Glo® 3/7 assay reagent (Promega Corporation) was added to each well at 24 h post-induction. The plates were incubated at ambient temperature for 2 h. Luminescence per well was measured with the FLUOstar Omega microplate reader (BMG Labtech). Mean luminescence readings per setup were calculated for each time-point and statistically analyzed.

Actin cytoskeleton staining. HCT116 and A549 cells were seeded into an 8-well chamber slide (Ibidi GmbH, Martinsried, Germany) and transfected after 24 h. The cells were fixed at 48 h post-transfection with 4% paraformaldehyde for 20 min. PBS was used to wash cells between steps. Cells were permeabilized using 0.1% Triton X-100 in 1X PBS for 15 min and blocked with 1% bovine serum albumin (BSA) in PBS for 20 min. For actin staining, the cells were incubated at a 1:100 dilution of tetramethylrhodamine-conjugated phalloidin (Invitrogen; Thermo Fisher Scientific, Inc.). The nuclei were counterstained with Hoechst 33258 (1 μg/μl). Stained cells were mounted in 70% glycerol and were visualized under an Olympus IX83 inverted fluorescence microscope (Olympus Corp.), using a red fluorescent filter ($\lambda_{ex}/\lambda_{em}$: 490/525 nm) to visualize filamentous actin structures, a blue fluorescent filter ($\lambda_{ex}/\lambda_{em}$: 355/465 nm) to visualize the nuclei, and a green fluorescent filter ($\lambda_{ex}/\lambda_{em}$: 490/525 nm) to visualize cells transfected with pmR-ZsGreen1.

Statistical analysis. Statistical analysis of data was performed using unpaired two-tailed t-test to measure differences between two setups. Analysis of variance with post-hoc Tukey's honestly significant difference (HSD) was used to test significant differences between multiple setups. Data from all quantitative experiments are presented as the mean ± standard deviation (SD). In all tests, significance value was defined as $P<0.05$, $P<0.01$ and $P<0.001$.

Results

Bioinformatics analysis predicts targeting of NF2-3'UTR by hsa-miR-92a-3p. To identify candidate miRNAs targeting the 3'UTR of the predominant *NF2* isoform 1 mRNA (NM_000268.3), the key characteristics of a functional miRNA:target interaction were analyzed. Context score percentile and aggregate preferentially conserved targeting scores (P_{CT}) of each miRNA binding site was provided by TargetScanHuman v6.2 (http://www.targetscan.org/vert_61/) (Table III). The thermodynamic stability of miRNA:target interaction was analyzed using PITA (http://genie.weizmann.ac.il/pubs/mir07/mir07_prediction.html). MirSVR scores predicting the likelihood of downregulation of *NF2* by miRNAs from sequence and structure characteristics of predicted miRNA binding sites were obtained from microRNA.org. Rank and target scores of miRNAs predicted to target *NF2*-3'UTR were analyzed by mirDB (http://mirdb.org/miRDB/). *In silico* analyses identified a phylogenetically conserved MRE for hsa-miR-92a-3p within the 3'UTR sequence of wild-type *NF2* (Fig. 1A). A summary of the bioinformatics analysis profiles of hsa-miR-92a-3p is presented in Table IV. Predictive scores of bioinformatics tools consistently ranked hsa-miR-92a-3p (hereinafter referred to as miR-92a) as a good potential candidate, and it was thus selected for the present study.

Dual-luciferase assays suggest negative regulation of NF2 by miR-92a via its 3'UTR. To test for endogenous regulation of *NF2* via its 3'UTR, a 792-bp segment of the *NF2*-3'UTR encompassing nucleotides 26-818 after the stop codon was cloned into the miRNA target expression vector pmirGLO (Promega Corporation) (Fig. 1A). Dual-Luciferase assays revealed a significant decrease in normalized firefly RLUs in HCT116 (Fig. 1B) and A549 (Fig. 1C) cells overexpressing wild-type *NF2*-3'UTR compared with cells transfected with the vector only, suggesting that *NF2* is endogenously regulated via its 3'UTR in both cell lines. Endogenous expression and significant overexpression of mature miR-92a from the pmR-ZsGreen1-miR-92a construct in HCT116 cells (Fig. 1D) and A549 cells (Fig. 1E) was verified and measured using the QuantiGene miRNA assay as described in Materials and methods. Co-transfection Dual-Luciferase assay results demonstrated a dose-dependent decrease in luciferase reporter expression corresponding to co-transfection of increasing amounts of miR-92a expression construct with wild-type *NF2*-3'UTR in both HCT116 (Fig. 1F) and A549 cells (Fig. 1G) under serum-depleted conditions.

To confirm the specificity of the interaction of miR-92a with its predicted binding site within the cloned *NF2*-3'UTR segment, dual-luciferase experiments were conducted using an *NF2*-3'UTR expression construct with mutated miR-92a MRE (Fig. 1H). Luciferase readouts from cells transiently overexpressing miR-92a and co-transfected with the mutant *NF2*-3'UTR were comparable to readouts from the empty vector controls in both HCT116 (Fig. 1I) and A549 cells (Fig. 1J), revealing that downregulation of luciferase reporter expression by miR-92a was reversed by destruction of its MRE within the *NF2*-3'UTR. Overall, these results demonstrated that miR-92a downregulated *NF2* via its 3'UTR, in part by directly interacting with its conserved MRE within the *NF2*-3'UTR sequence.

miR-92a downregulates endogenous NF2 mRNA and protein expression. MicroRNAs can regulate a gene either by causing mRNA degradation and/or by translational repression.

Table III. List of miRNA families targeting Human NF2 (NM_181833) 3'UTR broadly conserved among vertebrates.

	Conserved sites				Poorly conserved sites					
miRNA	Total	8mer	7mer-m8	7mer-1A	Total	8mer	7mer-m8	7mer-1A	Total context score	Aggregate PCT
miR-25/32/92abc/363/363-3p/367	1	0	1	0	1	0	1	0	-0.18	0.73
miR-7/7ab	0	0	0	0	3	0	3	0	-0.32	0.36
miR-223	0	0	0	0	2	0	0	2	-0.17	0.35
miR-15abc/16/16abc/195/322/424/497/1907	0	0	0	0	2	0	2	0	-0.08	0.24
miR-33a-3p/365/365-3p	0	0	0	0	1	0	0	1	-0.07	0.21
miR-31	0	0	0	0	2	0	2	0	-0.1	0.21
miR-34ac/34bc-5p/449abc/449c-5p	0	0	0	0	2	0	1	1	-0.17	0.18
miR-216b/216b-5p	0	0	0	0	2	0	2	0	-0.13	0.14
miR-383	0	0	0	0	1	0	0	1	-0.07	0.12
miR-143/1721/4770	0	0	0	0	1	0	0	1	-0.01	<0.1
miR-103a/107/107ab	0	0	0	0	1	0	1	0	-0.02	<0.1
miR-139-5p	0	0	0	0	1	0	0	1	-0.1	<0.1
miR-153	0	0	0	0	1	0	0	1	-0.01	<0.1
miR-183	0	0	0	0	1	0	1	0	-0.11	<0.1
miR-96/507/1271	0	0	0	0	1	0	1	0	-0.02	<0.1
miR-125a-5p/125b-5p/351/670/4319	0	0	0	0	2	0	0	2	-0.18	<0.1
miR-208ab/208ab-3p	0	0	0	0	1	0	0	1	-0.01	<0.1
miR-193/193b/193a-3p	0	0	0	0	1	1	0	0	-0.38	<0.1
miR-146ac/146b-5p	1	0	1	0	0	0	0	0	-0.19	<0.1
miR-24/24ab/24-3p	0	0	0	0	3	0	0	3	-0.03	<0.1
miR-10abc/10a-5p	0	0	0	0	2	0	2	0	-0.12	<0.1
miR-93/93a/105/106a/291a 3p/294/295/302abcde/372/373/428/519 a/520be/520acd-3p/1378/1420ac	0	0	0	0	1	0	1	0	-0.02	<0.1
miR-499-5p	0	0	0	0	1	0	0	1	-0.01	<0.1
miR-9/9ab	0	0	0	0	1	0	0	1	-0.01	<0.1
miR-22/22-3p	0	0	0	0	2	0	2	0	-0.18	<0.1
miR-130ac/301ab/301b/301b 3p/454/721/4295/3666	0	0	0	0	1	0	1	0	-0.03	<0.1
miR-122/122a/1352	0	0	0	0	1	0	0	1	-0.1	<0.1

Several miRNA families were predicted to have binding sites broadly conserved among vertebrates within the *NF2*-3'UTR sequence. Of these, the binding sites for hsa-miR-92a-1 (NR_029508.1) ranked highest according to aggregate preferentially conserved targeting (P_{CT}) scores. *NF2*, neurofibromin 2.

Table IV. Summary of bioinformatics analysis profiles of hsa-miR-92a.

miRNA	# of MREs within *NF2*-3'UTR	MRE position	ΔΔG (kcal/mol)	Context score percentile	P_{CT}	MirSVR score and rank	mirDB target score and rank
hsa-miR-92a	2	159-165[a]	-4.43	81	0.72	-0.1779 (rank 5)	52 (rank 146)
		2,816-2,822	-12.57	8	<0.1	-	-

[a]Conserved site, broadly conserved among vertebrates. *NF2*, neurofibromin 2; UTR, untranslated region; MRE, microRNA response element; P_{CT}, preferentially conserved targeting scores.

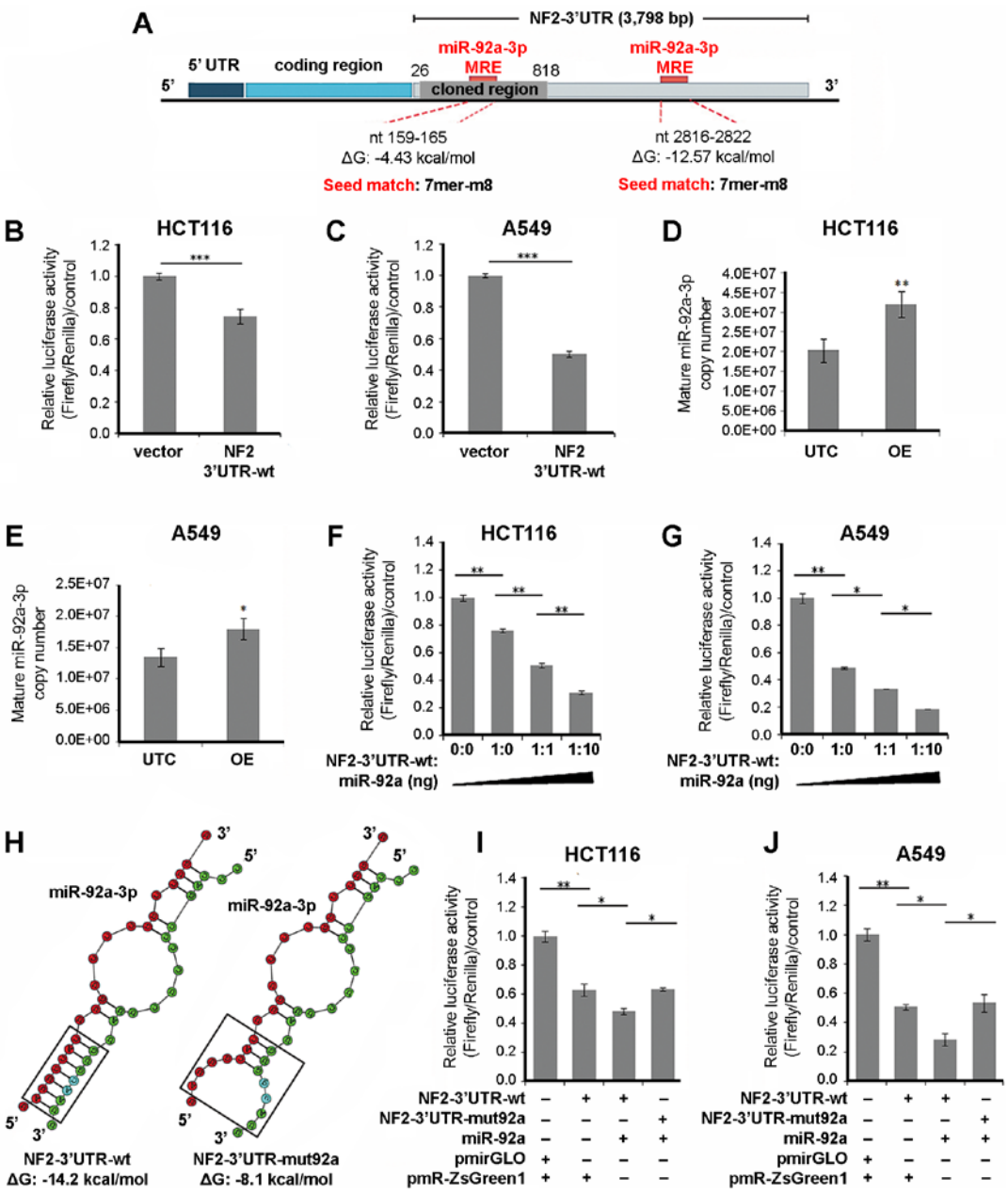

Figure 1. *NF2* is downregulated by miR-92a-3p via its 3'UTR. (A) Schematic representation of the full and cloned 3'UTR region of *NF2* isoform I mRNA and the predicted miR-92a-3p MREs within its sequence. Dual-Luciferase assay of (B) HCT116 and (C) A549 cells transfected with empty vector (i.e., pmirGLO) or *NF2*-3'UTR-wild-type. (D and E) The expression levels of mature miR-92a-3p were measured by QuantiGene miRNA assay in untransfected (UTC) or miR-92a construct-transfected (OE) HCT116 and A549 cells. Dual-Luciferase assay of (F) HCT116 and (G) A549 cells co-transfected with increasing plasmid ratios of *NF2*-3'UTR-wild-type:miR-92a. (H) Secondary structure analysis of the RNA-RNA interaction (boxed region) between miR-92a-3p (red) and its MRE within wild-type vs. mutant *NF2*-3'UTR (green). Dual-Luciferase assay of (I) HCT116 and (J) A549 cells co-transfected with wild-type or miR-92a-3p MRE mutant *NF2*-3'UTR and miR-92a expression vectors. All experiments were performed in cells maintained in 0.5% serum. Data presented are representative of three independent trials and expressed as the mean ± standard deviation (SD). *P≤0.05, **P≤0.01, ***P≤0.001. *NF2*, neurofibromin 2; UTR, untranslated region; MRE, microRNA response element.

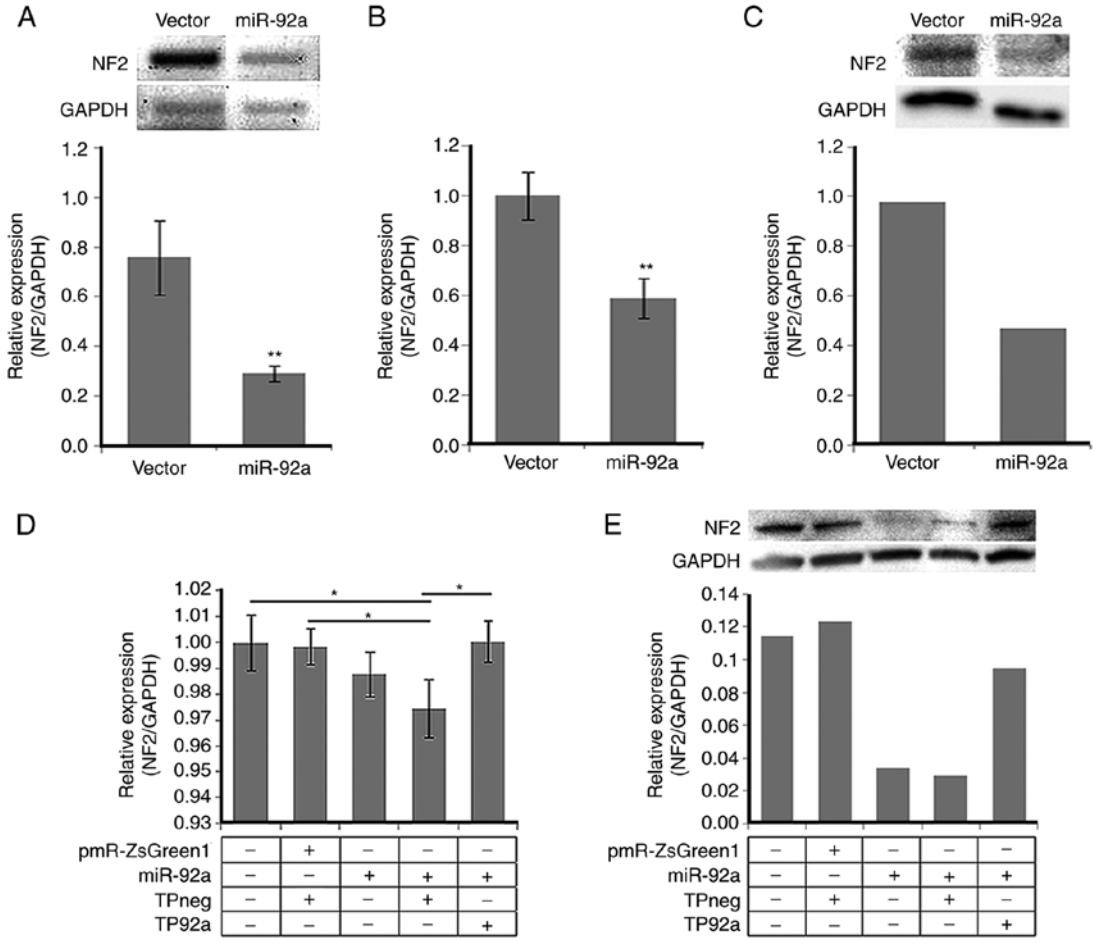

Figure 2. miR-92a-3p downregulates NF2 mRNA and protein expression by interacting with its conserved MRE within the *NF2*-3'UTR. (A) Semi-quantitative reverse transcription-polymerase chain reaction (semi-RT-qPCR), (B) quantitative RT-PCR (RT-qPCR) and (C) western blotting detection of *NF2*/Merlin expression levels in HCT116 cells transfected with empty vector or miR-92a expression construct. (D) RT-qPCR and (E) western blotting detection of *NF2*/Merlin expression in HCT116 cells co-transfected with pmR-ZsGreen1 and negative control target protector (TPneg), or with miR-92a expression construct and miR-92a-target protector (TP-92a). All experiments were performed in cells maintained in 0.5% serum. Data presented are representative of three independent trials and expressed as the mean ± standard deviation (SD). $^{*}P \leq 0.05$, $^{**}P \leq 0.01$. *NF2*, neurofibromin 2; UTR, untranslated region; MRE, microRNA response element.

Semi-RT-qPCR results revealed significant downregulation of *NF2* mRNA expression in HCT116 cells overexpressing miR-92a compared with cells transfected with empty vector under serum-deprived conditions (Fig. 2A), which corroborated with the results obtained in parallel RT-qPCR experiments (Fig. 2B). Western blot analyses of transfected HCT116 cells also revealed markedly lower Merlin protein expression levels in cells transiently overexpressing miR-92a vs. the empty vector control (Fig. 2C). These results suggest that miR-92a can downregulate *NF2* expression at both the mRNA and protein level, either through transcript degradation alone, or through translational repression as well.

Typically, miRNAs target multiple mRNAs within the cell via partial seed sequence complementarity with their respective 3'UTRs. To demonstrate that the regulatory effects of miR-92a overexpression on *NF2* mRNA and protein expression is due to direct interaction of miR-92a with *NF2*-3'UTR, a target protector oligonucleotide (TP-92a) was used to specifically block the conserved MRE of miR-92a within the *NF2*-3'UTR. HCT116 cells transfected with miR-92a alone or co-transfected with a negative control target protector (TPneg) displayed significantly downregulated *NF2* mRNA expression compared with control cells transfected with empty vector and TPneg. This negative regulatory effect was abolished upon co-transfection of miR-92a with TP-92a (Fig. 2D). Similarly, co-transfection of miR-92a with TP-92a rescued the expression of Merlin, which was downregulated in cells transfected with miR-92a alone or co-transfected with TPneg (Fig. 2E). Overall, these results demonstrated that miR-92a downregulates *NF2* mRNA and protein expression specifically by binding to its conserved MRE within the *NF2*-3'UTR sequence.

miR-92a promotes cell proliferation and inhibits cell apoptosis. Merlin is known to be involved in contact-mediated inhibition of proliferation (2,3). To determine whether upregulation of miR-92a can override this function of Merlin, proliferation rates were assessed in HCT116 and A549 cells transfected with miR-92a expression construct. Under serum-depleted conditions (2%), HCT116 (Fig. 3A) and A549 (Fig. 3B) cells overexpressing miR-92a exhibited a significant increase in the number of viable cells between 72 and 96 h post-transfection, at which point the cells were observed to reach semi-confluence (>90% growth surface area). This indicated that, under space-limiting conditions, overexpression of miR-92a

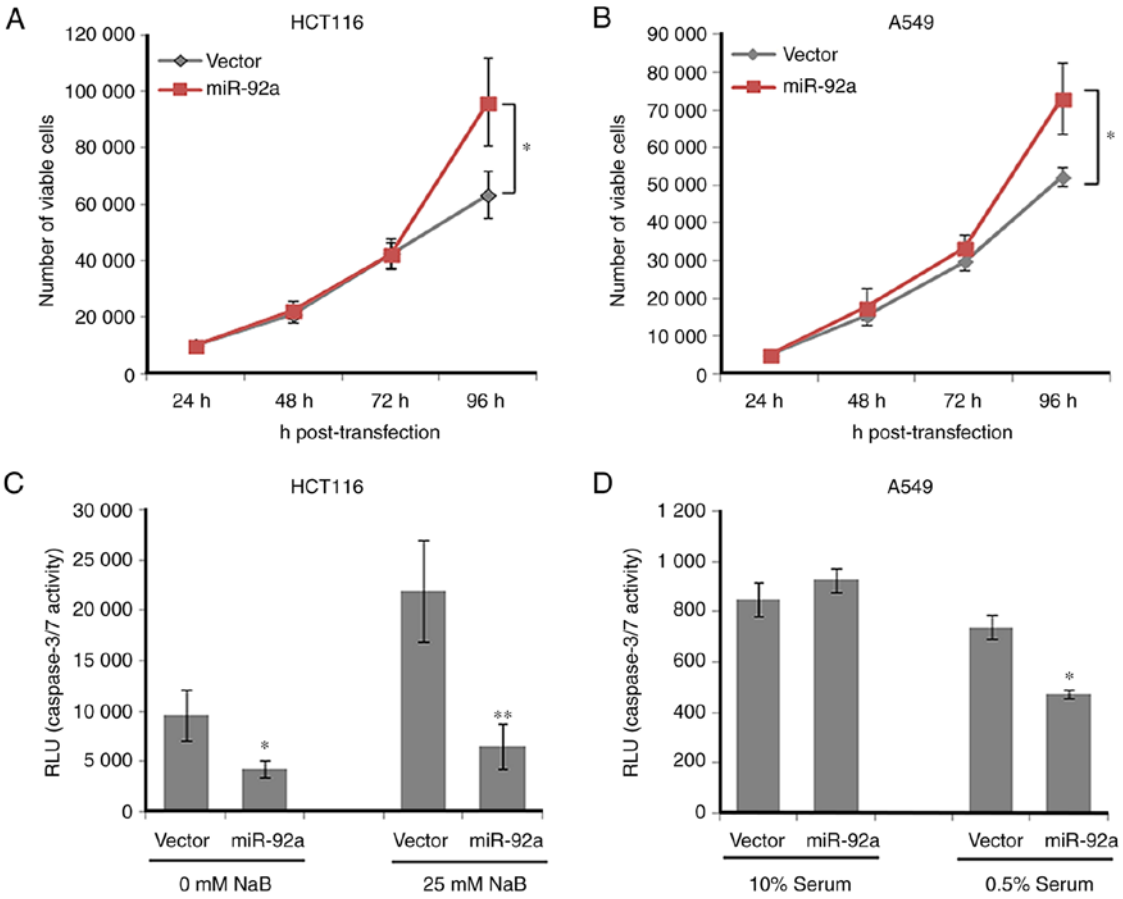

Figure 3. Overexpression of miR-92a-3p enhances cell proliferation and inhibits apoptosis induction of HCT116 and A549 cells. Proliferation of (A) HCT116 and (B) A549 cells transfected with empty vector (i.e., pmR-ZsGreen1) or miR-92a expression construct in 0.5% serum. (C) Caspase-3/7 activity in HCT116 cells transfected with miR-92a expression construct and maintained in 2% serum, with or without the presence of sodium butyrate (NaB). (D) Caspase-3/7 activity in A549 cells transfected with miR-92a expression construct maintained in 10 or 0.5% serum. Data presented are representative of three independent trials and expressed as the mean ± standard deviation (SD). $^{*}P \leq 0.05$, $^{**}P \leq 0.01$.

promoted proliferation of HCT116 and A549 cells, at least in part through downregulation of *NF2* mRNA/protein expression.

Merlin also exerts its tumor suppressor effects by promoting apoptosis via the Hippo/SWH (Sav/Wts/Hpo) signaling pathway (14). Assessment of apoptosis induction in HCT116 cells transfected with miR-92a and maintained under low-serum conditions (2%) revealed significantly lower levels of activated caspase-3/7 compared with empty vector control in both the absence or presence of the apoptosis inducer sodium butyrate (Fig. 3C). Similarly, overexpression of miR-92a in A549 cells incubated under serum-deprived conditions (0.5%) was associated with significantly lower levels of active caspase-3/7 compared with empty vector control (Fig. 3D). Overall, these results demonstrated that miR-92a inhibited caspase-3/7 activation and promoted resistance to apoptosis in HCT116 and A549 cells, possibly, at least in part, by downregulation of *NF2* mRNA/protein expression.

miR-92a promotes cell migration. To assess whether overexpression of miR-92a inhibits the negative regulatory effect of Merlin on cell motility, the wound healing capacity of transfected HCT116 and A549 cells was assessed. Cells overexpressing miR-92a migrated over the introduced wound gap at a significantly faster rate compared with cells transfected with empty vector control in both HCT116 (Fig. 4A) and A549 (Fig. 4B) cell lines under serum-depleted conditions (2%). This indicated that overexpression of miR-92a enhanced the motility of colorectal and lung cancer cells, possibly in part by inhibition of *NF2* mRNA/protein expression.

miR-92a promotes epithelial-mesenchymal transition (EMT). To explore a possible molecular mechanism underlying the observed increase in the migration capacity of cells overexpressing miR-92a, the expression of EMT markers was assessed. At the transcriptional level, normalized band intensities from semi-RT-qPCR consistently showed downregulation of *NF2* mRNA expression in cells transfected with miR-92a vs. empty vector control (Fig. 4C). Consequently, a decrease in the transcript expression of the epithelial marker E-cadherin was observed in miR-92a-overexpressing cells, with a corresponding increase in mRNA expression of the mesenchymal marker N-cadherin (Fig. 4C). Contrary to what was expected, a decrease in the mRNA expression of vimentin was observed in miR-92a-overexpressing cells (Fig. 4C). At the protein level, normalized band intensities from western blot analyses revealed downregulation of *NF2* protein expression in cells transfected with miR-92a compared with empty vector control (Fig. 4D). No significant change in E-cadherin protein expression was observed in cells overexpressing

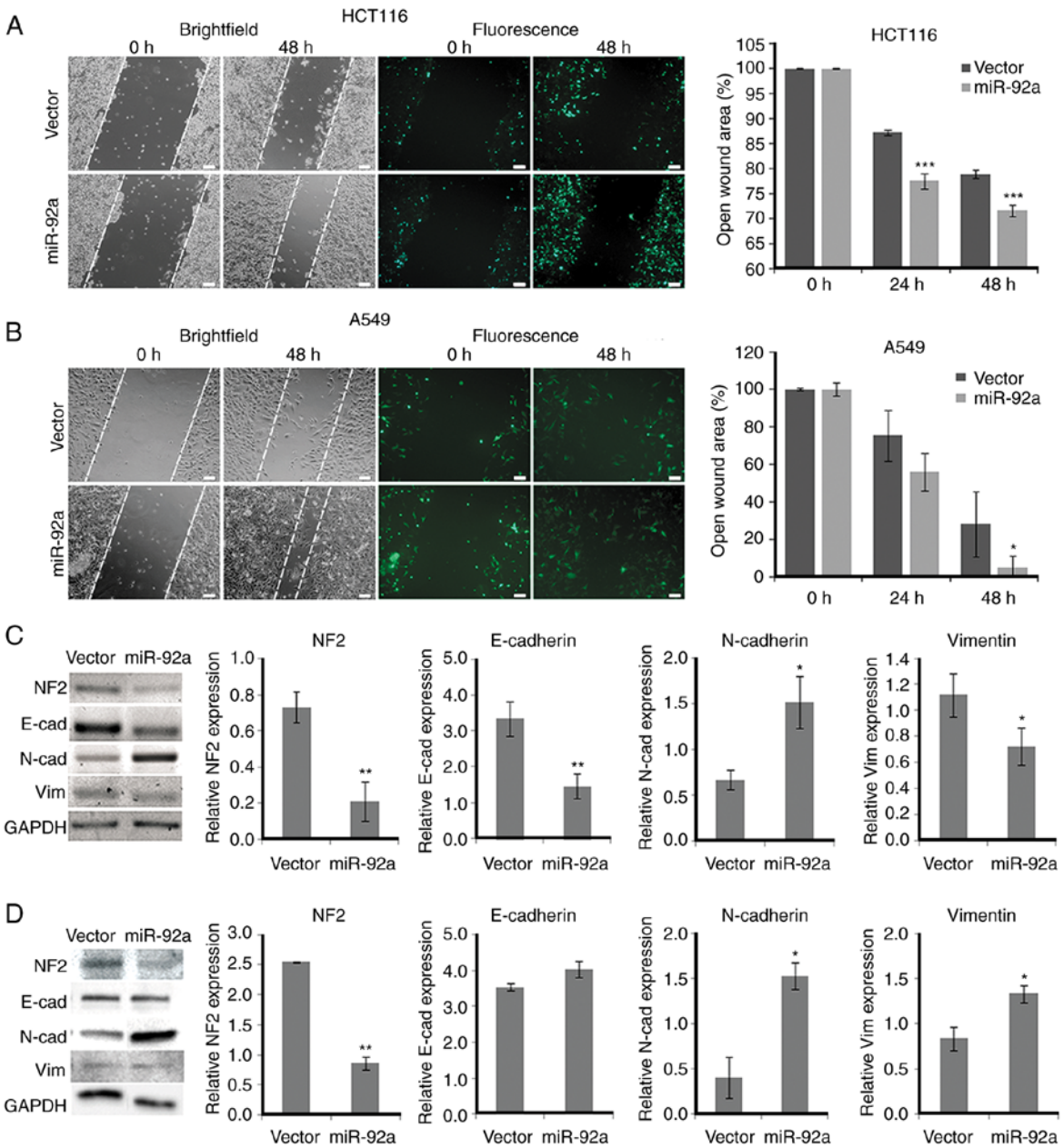

Figure 4. Overexpression of miR-92a-3p enhances the motility of HCT116 and A549 cells. Representative micrographs of (A) HCT116 and (B) A549 wound fields after scratching (0 h) the monolayer and at 24 h post-scratch. Scale bars, 100 μm. Percent open wound of the field view area occupied by cells at 24 and 48 h post-scratch vs. time-point 0 h is shown. (C) Semi-quantitative reverse transcription-polymerase chain reaction (semi-RT-PCR) and (D) western blotting detection of *NF2*/Merlin and EMT marker (E-cadherin, N-cadherin and vimentin) expression levels in HCT116 cells transfected with vector or miR-92a expression construct. The lysates used for western blotting were from the same independent trial shown in Fig. 2C. Data presented are representative of three independent trials and expressed as the mean ± standard deviation (SD). *P≤0.05, **P≤0.01, ***P≤0.001. EMT, epithelial-mesenchymal transition.

miR-92a, although a marked increase in protein expression of both N-cadherin and vimentin was detected (Fig. 4D). Overall, these results demonstrated that downregulation of *NF2* by overexpression of miR-92a led to an apparent shift in EMT marker expression from an epithelial to a mesenchymal-like phenotype. These results were consistent with the observed increase in the migration capacity of cells overexpressing miR-92a, demonstrating that negative regulation of *NF2* by miR-92a in HCT116 cells promoted cell migration by inducing partial EMT.

miR-92a alters F-actin cytoskeletal organization by targeting NF2. Merlin is known to act as an organizer of the actin cytoskeleton primarily through the F1 and F2 subdomains within its N-terminal 4.1 ezrin-radixin-moesin (FERM) domain. Although not required *per se*, the domains also facilitate the function of Merlin in contact-inhibition of growth (15). To determine whether miR-92a overexpression exerts deleterious effects on the cytoskeletal dynamics of epithelial carcinoma cells, the filamentous actin network of transfected A549 cells was visualized through fluorescence staining.

Untransfected A549 cells displayed a typical resting epithelial cell morphology, with an overall flat, spread-out cell shape, sparse transverse stress fibers and high intercellular cohesion, as also observed in control cells transfected

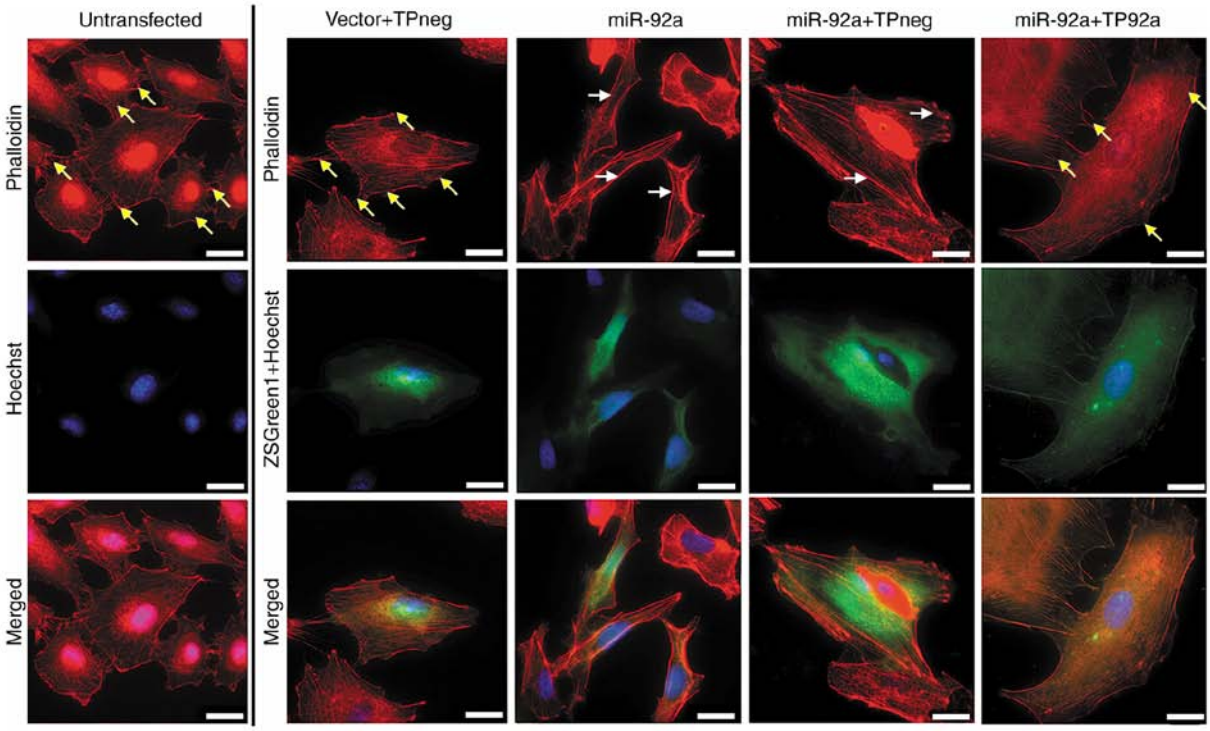

Figure 5. Overexpression of miR-92a-3p alters the cytoskeletal organization of A549 cells. Fluorescent images showing the F-actin cytoskeletal organization of A549 cells co-transfected with empty vector (i.e., pmiR-ZsGreen1) or miR-92a expression construct and TPneg or TP92a. Yellow arrows indicate cells with sparse transverse actin filaments with a high number of intercellular adhesions. White arrows indicate cells with dense and prominent transverse F-actin fibers and formation of multiple pseudopodia, which is characteristic of motile cells (phalloidin: F-actin; Hoechst: nuclei, ZsGreen1: cells positively transfected with pmR-ZsGreen1). Scale bars, 25 μm.

with empty pmR-ZsGreen1 vector and negative control target protector oligonucleotide (Fig. 5). By contrast, A549 cells transfected with miR-92a alone or co-transfected with negative control target protector displayed gross morphological changes in cytoskeletal organization, as evidenced by cytoplasmic shrinkage and a spindle-like morphology, which are characteristic of highly motile cells (Fig. 5). Co-transfection of miR-92a with the target protector for its conserved MRE within *NF2*-3'UTR appeared to abolish the cytoskeletal changes induced by miR-92a overexpression (Fig. 5). Collectively, these results indicated that miR-92a induced a highly dynamic actin network typical of cells with a more motile phenotype, possibly in part through downregulation of *NF2* mRNA/protein expression.

Knockdown of NF2 by siRNA phenocopies oncogenic effects of miR-92a overexpression. MicroRNAs target multiple genes within the cell via partial seed sequence complementarity with their respective 3'UTRs. Thus, phenotypic readouts observed upon overexpression of a single miRNA species is typically the overall effect of the miRNA on its endogenous targets expressed in the cell system tested. To confirm the contribution of *NF2* knockdown in the observed phenotypes consequent to miR-92a overexpression, RNA interference via small interfering RNA (siRNA) was used as a gene-specific alternative to knockdown by a miRNA. An *NF2*-specific pre-designed siRNA oligonucleotide was used to induce short-term silencing of the *NF2* gene. Knockdown of endogenous NF2 was confirmed by RT-qPCR (Fig. 6A) and western blot analysis (Fig. 6B).

Similar to cells transiently overexpressing miR-92a, cell proliferation experiments performed on HCT116 (Fig. 6C) and A549 (Fig. 6D) cells revealed a marked increase in the number of viable cells in setups transfected with *NF2* siRNA upon reaching semi-confluence (>90%) at 24 h post-transfection. Abolition of the pro-apoptotic function of Merlin was demonstrated in A549 cells by the significantly lower activity of caspase-3/7 measured in cells transfected with *NF2* siRNA compared with control cells (Fig. 6F). On the other hand, *NF2* siRNA-transfected HCT116 cells did not display any significant difference in caspase-3/7 activity compared with controls (Fig. 6E). This finding suggests that the function of Merlin in promoting apoptosis is cell context-dependent.

Knockdown of Merlin by transfection of *NF2* siRNA also resulted in a significant increase in motility compared with controls for both HCT116 (Fig. 6G) and A549 (Fig. 6H) cells. Furthermore, HCT116 cells transfected with *NF2* siRNA consequently exhibited a decrease in the expression of E-cadherin with a concurrent increase in the mRNA expression of N-cadherin and vimentin at both the mRNA (Fig. 6I) and protein levels (Fig. 6J). Additionally, A549 cells transfected with *NF2* siRNA displayed gross morphological changes brought about by cytoskeletal organization, as evidenced by cytoplasmic shrinkage and a more spindle-like morphology, which are characteristic of highly motile cells (Fig. 6K).

Overall, these results demonstrated that *NF2* knockdown by RNA interference phenocopies the oncogenic effects of miR-92a overexpression. Given that miR-92a has also been shown to exert its oncogenic effects in colorectal and lung cancer by potentially targeting phosphatase and

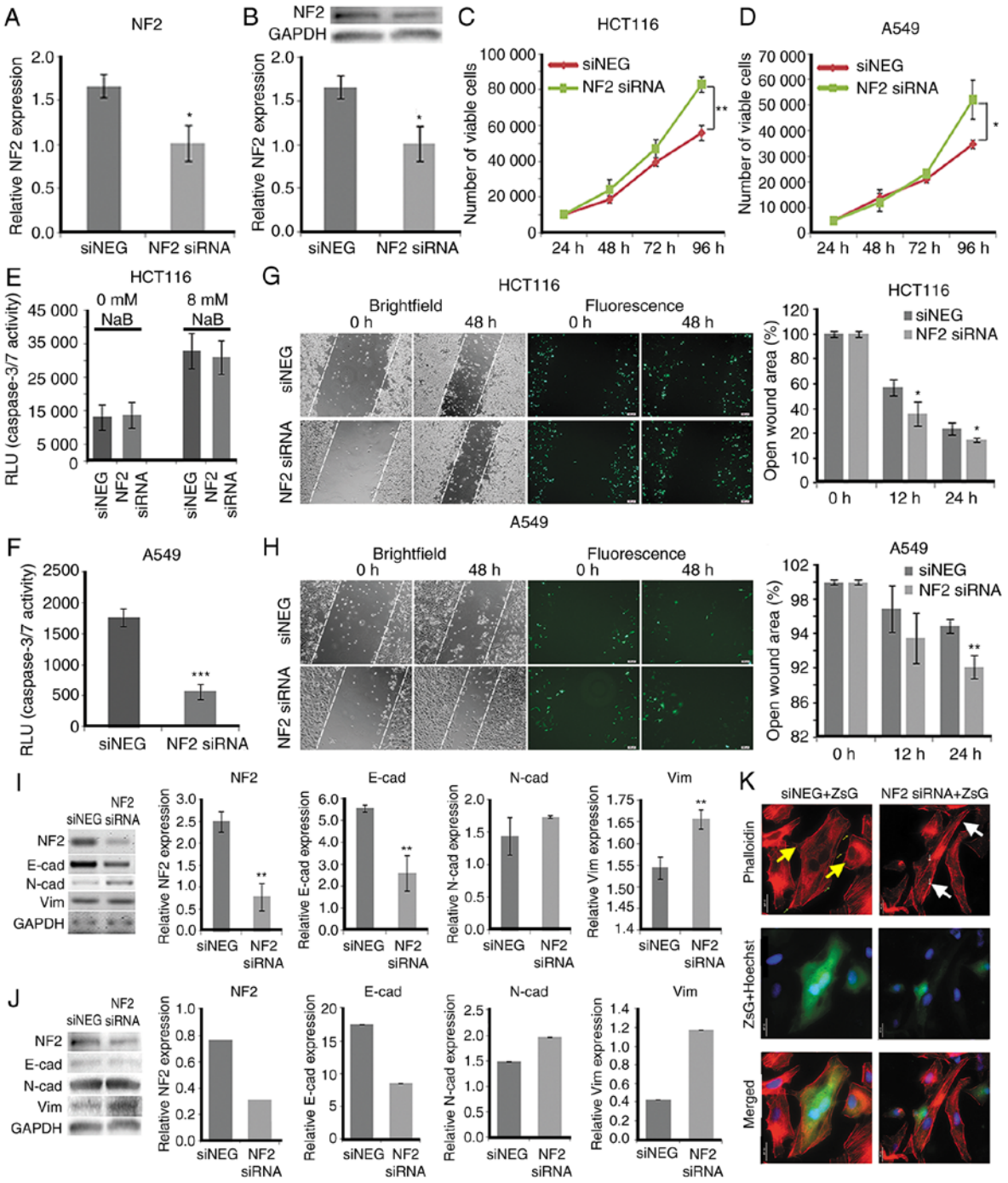

Figure 6. siRNA-mediated *NF2* silencing phenocopies pro-oncogenic effects of miR-92a-3p overexpression. (A) Reverse transcription-quantitative polymerase chain reaction (RT-qPCR) and (B) western blotting detection of *NF2*/Merlin expression in HCT116 cells transfected with negative control siRNA (siNEG) or *NF2* siRNA. Proliferation of (C) HCT116 and (D) A549 cells transfected with siNEG or *NF2* siRNA. Caspase-3/7 activity of (E) HCT116 and (F) A549 cells transfected with siNEG or *NF2* siRNA. Representative micrographs of (G) HCT116 and (H) A549 wound fields after scratching (0 h) the monolayer and at 24 h post-scratch. Scale bars, 100 μm. (I) Semi-RT-qPCR and (J) western blotting detection of *NF2*/Merlin and EMT marker expression levels in HCT116 cells transfected with siNEG or *NF2* siRNA. Data are expressed as the mean ± standard deviation (SD). *P≤0.05, **P≤0.01, ***P≤0.001. (K) Fluorescent images showing the F-actin cytoskeletal organization of A549 cells co-transfected with pmR-ZsGreen1 and siNEG or *NF2* siRNA. Yellow arrows indicate cells with sparse transverse actin filaments with a high number of intercellular adhesions. White arrows indicate cells with dense and prominent transverse F-actin fibers and formation of multiple pseudopodia, characteristic of motile cells (phalloidin: F-actin; Hoechst: nuclei, ZsGreen1: cells positively transfected with pmR-ZsGreen1). Scale bar, 25 μm. *NF2*, neurofibromin 2; EMT, epithelial-mesenchymal transition.

tensin homolog (PTEN) (16,17) and Krüppel-like factor 4 (KLF4) (18), the results of the present study confirm the role of miR-92a in simultaneously targeting the tumor suppressors *NF2*, PTEN and KLF4, and possibly other targets, in order to bring about a congruent phenotypic readout.

Discussion

Until recently, inactivation or mutations of neurofibromin 2 gene (*NF2*) have not attracted attention in cancer, since they are not as frequently observed in common human

malignancies. When present, however, they can affect disease progression, aggressiveness and prognosis. In prostate cancer, for example, inactivation of *NF2* has been associated with increased invasiveness and chemoresistance (19,20). In glioblastoma multiforme, a particularly aggressive type of brain tumor, Merlin expression was found to be reduced in up to 61% (n=23) of the cases (21).

Notably, deficiency in the expression levels of the tumor suppressor protein Merlin frequently occurs in multiple cancer types at a rate higher compared with what can be predicted by mutational analysis of the *NF2* gene (10). The molecular mechanisms responsible for this remain elusive and the consequences of Merlin downregulation in cancer progression have only recently started to become unraveled. In the absence of inactivating mutations in *NF2*, post-translational modifications, such as Merlin phosphorylation, and epigenetic regulation, such as *NF2* promoter methylation, were documented to be altered in certain types of cancer (4,8,9). Loss of Merlin in breast, pancreatic and colorectal cancers was correlated with tumor grade and enhanced activation of the RAS pathway (8,22,23). While post-translational and epigenetic regulation may account for the disparity between the lack of mutations in *NF2* and low Merlin expression in such cases, these mechanisms have not been consistently observed across different types of cancer (10). This warrants an investigation of other molecular mechanisms that may contribute to Merlin downregulation.

The altered expression of oncogenes, tumor suppressor genes and cell cycle regulatory genes due to miRNA regulation is known to contribute to tumorigenesis (11,24). In the present study, the ability of miRNAs to target and regulate *NF2* expression via its 3'UTR was investigated. In particular, it was hypothesized that loss of Merlin expression in colorectal and non-small cell lung cancer (*NSCLC*) may be due in part to negative regulation by miR-92a, which is upregulated in these cancer types (17,18). This was supported by results obtained in luciferase reporter assays, wherein a significant decrease in luciferase activity was observed when wild-type *NF2*-3'UTR reporter construct was co-transfected with miR-92a. Mutation of this evolutionarily conserved miR-92a seed sequence abolished repression. Furthermore, RT-qPCR and western blot analyses confirmed that miR-92a can downregulate the endogenous *NF2* target by binding to this seed sequence. This was validated by target protection experiments, thus, confirming the accessibility of this seed sequence within *NF2*-3'UTR to miR-92a targeting.

In the present study, overexpression of exogenous miR-92a in HCT116 and A549 cells resulted in a marked increase in proliferation and migration abilities, as well as resistance to apoptosis. This is in agreement with previous data revealing that miR-92a may play an oncogenic role in colorectal (25,26) and lung cancer (17) cell lines and tissues. miR-92a expression in HCT116 and A549 cells was found to be significantly higher compared with their normal cell line counterparts, FHC and BEAS-2B (16,17). Merlin expression, on the other hand, has been revealed to be significantly lower in colorectal and lung cancer cells (4,8). The expression levels of miR-92a in these types of cancer have been shown to be correlated with their propensity for metastasis (17,26). Collectively, these findings along with the luciferase assays and target protector control experiments, indicated that miR-92a contributed, at least partially, to the phenotypic readouts observed by direct targeting of the *NF2*-3'UTR.

Overexpression of exogenous miR-92a in epithelial A549 cells was also found to result in gross changes in actin cytoskeletal architecture of transfected cells, which assumed a more motile phenotype. This suggests that direct targeting of the *NF2*-3'UTR by miR-92a inhibits not only its tumor suppressor function, but also its independent role as an organizer of the actin cytoskeleton (15). Merlin deficiency was recently revealed to prime the membrane:cytoskeleton interface for macropinocytosis resulting in profound alteration of epithelial growth factor receptor trafficking in the cell (27). Therefore, the results of the present study suggest that miR-92a regulation of the *NF2* gene via its 3'UTR can alter the F-actin cytoskeletal organization of cancer cells and it may directly affect membrane receptor recycling dynamics and downstream signaling cascades through this mechanism.

Knockdown experiments using siRNA decoupled the specific contribution of *NF2* knockdown to the pro-oncogenic readouts of miR-92a overexpression. In contrast to the miRNA overexpression experiments, wherein multiple genes may be targeted by a single miRNA, knockdown by *NF2*-specific siRNA served as a surrogate to elucidate the phenotype of miR-92a-mediated targeting of *NF2*. In all phenotypic assays performed in the present study, knockdown using siRNA phenocopied the effects of miR-92a downregulation of *NF2*.

The oncogenic role of miR-92a in colorectal and lung cancer cells has previously been revealed to be partially mediated by its downregulation of the PTEN tumor suppressor gene (17,28) and the KLF4 transcription factor (18). The expression of PTEN was found to be inversely correlated with miR-92a expression in colorectal and lung cancer tissues (16,17,28). Similar to PTEN, *NF2* is a tumor suppressor that negatively regulates the phosphatidylinositol 3-kinase/protein kinase B (PI3K/Akt) pathway by binding to PI3K enhancer-L (PIKE-L), thereby preventing its coupling to and activation of PI3K (29,30). This suggests that the PI3K/Akt pathway is inhibited by miR-92a in colorectal and lung cancer cells, at least in part by downregulation of PTEN and its co-target Merlin. In colorectal cancer cells, upregulation of miR-92a was found to promote cell proliferation and migration through direct targeting of KLF4 (18).

In conclusion, the findings of the present study demonstrated the oncogenic role of miR-92a deregulation in cancer, mediated in part by its negative regulation of the tumor-suppressive functions of Merlin through direct targeting of *NF2*-3'UTR. Overall, the findings from the present study confirm Merlin as a target of miR-92a, expanding its function as an oncogenic miRNA in colorectal and non-small cell lung cancer.

Acknowledgements

Not applicable.

Funding

The present study was supported by grants from the University of the Philippines System (OVPAA-EIDR Code 06-008) and the Philippine Council for Health Research and Development (grant code. FP150025).

Availability of data and materials

The datasets used and/or analyzed in the present study are available from the corresponding author upon reasonable request. Raw data and gene constructs used in the study are available from the corresponding author upon reasonable request.

Authors' contributions

KMMA and RLG conceived and designed the study, developed the methodology, analysed and interpreted the data, wrote, reviewed and revised the manuscript. KMMA performed all the experiments and organized all data and RLG determined the scope of the study and provided overall supervision. Both authors read and approved the manuscript and agree to be accountable for all aspects of the research in ensuring that the accuracy or integrity of any part of the work are appropriately investigated and resolved.

Ethics approval and consent to participate

Not applicable.

Patient consent for publication

Not applicable.

Competing interests

The authors declare that they have no competing interests.

References

1. Gutmann DH, Hirbe AC and Haipek CA: Functional analysis of neurofibromatosis 2 (NF2) missense mutations. Hum Mol Genet 10: 1519-1529, 2001.
2. Schroeder RD, Angelo LS and Kurzrock R: NF2/Merlin in hereditary neurofibromatosis 2 versus cancer: Biologic mechanisms and clinical associations. Oncotarget 5: 67-77, 2014.
3. Curto M and McClatchey AI: Nf2/Merlin: A coordinator of receptor signalling and intercellular contact. Br J Cancer 98: 256-262, 2008.
4. Morrow KA and Shevde LA: Merlin: The wizard requires protein stability to function as a tumor suppressor. Biochim Biophys Acta 1826: 400-406, 2012.
5. Evans DG: Neurofibromatosis type 2 (NF2): A clinical and molecular review. Orphanet J Rare Dis 4: 16, 2009.
6. Petrilli AM and Fernández-Valle C: Role of Merlin/NF2 inactivation in tumor biology. Oncogene 35: 537-548, 2015.
7. Yoo NJ, Park SW and Lee SH: Mutational analysis of tumour suppressor gene NF2 in common solid cancers and acute leukaemias. Pathology 44: 29-32, 2012.
8. Čačev T, Aralica G, Lončar B and Kapitanović S: Loss of NF2/Merlin expression in advanced sporadic colorectal cancer. Cell Oncol 37: 69-77, 2014.
9. Morrow KA, Das S, Metge BJ, Ye K, Mulekar MS, Tucker JA, Samant RS and Shevde LA: Loss of tumor suppressor Merlin in advanced breast cancer is due to post-translational regulation. J Biol Chem 286: 40376-40385, 2011.
10. Quan M, Cui J, Xia T, Jia Z, Xie D, Wei D, Huang S, Huang Q, Zheng S and Xie K: Merlin/NF2 suppresses pancreatic tumor growth and metastasis by attenuating the FOXM1-mediated Wnt/β-catenin signaling. Cancer Res 75: 4778-4789, 2015.
11. Jansson MD and Lund AH: MicroRNA and cancer. Mol Oncol 6: 590-610, 2012.
12. Wang X: Improving microRNA target prediction by modeling with unambiguously identified microRNA-target pairs from CLIP-ligation studies. Bioinformatics 32: 1316-1322, 2016.
13. Gebäck T, Schulz MM, Koumoutsakos P and Detmar M: TScratch: A novel and simple software tool for automated analysis of monolayer wound healing assays. Biotechniques 46: 265-274, 2009.
14. Hamaratoglu F, Willecke M, Kango-Singh M, Nolo R, Hyun E, Tao C, Jafar-Nejad H and Halder G: The tumour-suppressor genes *NF2*/*Merlin* and *Expanded* act through Hippo signalling to regulate cell proliferation and apoptosis. Nat Cell Biol 8: 27-36, 2006.
15. Lallemand D, Saint-Amaux AL and Giovannini M: Tumor-suppression functions of merlin are independent of its role as an organizer of the actin cytoskeleton in Schwann cells. J Cell Sci 122: 4141-4149, 2009.
16. Zhang G, Zhou H, Xiao H, Liu Z, Tian H and Zhou T: MicroRNA-92a functions as an oncogene in colorectal cancer by targeting PTEN. Dig Dis Sci 59: 98-107, 2014.
17. Ren P, Gong F, Zhang Y, Jiang J and Zhang H: MicroRNA-92a promotes growth, metastasis, and chemoresistance in non-small cell lung cancer cells by targeting PTEN. Tumor Biol 37: 3215-3225, 2016.
18. Lv H, Zhang Z, Wang Y, Li C, Gong W and Wang X: MicroRNA-92a promotes colorectal cancer cell growth and migration by inhibiting KLF4. Oncol Res 23: 283-290, 2016.
19. Kawana Y, Ichikawa T, Suzuki H, Ueda T, Komiya A, Ichikawa Y, Furuya Y, Akakura K, Igarashi T and Ito H: Loss of heterozygosity at 7q31.1 and 12p13-12 in advanced prostate cancer. Prostate 53: 60-64, 2002.
20. Malhotra A, Shibata Y, Hall IM and Dutta A: Chromosomal structural variations during progression of a prostate epithelial cell line to a malignant metastatic state inactivate the NF2, NIPSNAP1, UGT2B17, and LPIN2 genes. Cancer Biol Ther 14: 840-852, 2013.
21. Lau YK, Murray LB, Houshmandi SS, Xu Y, Gutmann DH and Yu Q: Merlin is a potent inhibitor of glioma growth. Cancer Res 68: 5733-5742, 2008.
22. Bakker AC, La Rosa S, Sherman LS, Knight P, Lee H, Pancza P and Nievo M: Neurofibromatosis as a gateway to better treatment for a variety of malignancies. Prog Neurobiol 152: 149-165, 2017.
23. Couderc C, Boin A, Fuhrmann L, Vincent-Salomon A, Mandati V, Kieffer Y, Mechta-Grigoriou F, Del Maestro L, Chavrier P, Vallerand D, *et al*: AMOTL1 promotes breast cancer progression and is antagonized by Merlin. Neoplasia 18: 10-24, 2016.
24. Li M, Guan X, Sun Y, Mi J, Shu X, Liu F and Li C: miR-92a family and their target genes in tumorigenesis and metastasis. Exp Cell Res 323: 1-6, 2014.
25. Yamada N, Nakagawa Y, Tsujimura N, Kumazaki M, Noguchi S, Mori T, Hirata I, Maruo K and Akao Y: Role of intracellular and extracellular microRNA-92a in colorectal cancer. Transl Oncol 6: 482-492, 2013.
26. Zhou T, Zhang G, Liu Z, Xia S and Tian H: Overexpression of miR-92a correlates with tumor metastasis and poor prognosis in patients with colorectal cancer. Int J Colorectal Dis 28: 19-24, 2013.
27. Chiasson-Mackenzie C, Morris ZS, Liu CH, Bradford WB, Koorman T and McClatchey AI: Merlin/ERM proteins regulate growth factor-induced macropinocytosis and receptor recycling by organizing the plasma membrane: Cytoskeleton interface. Genes Dev 32: 1201-1214, 2018.
28. Ke TW, Wei PL, Yeh KT, Chen WT and Cheng YW: MiR-92a promotes cell metastasis of colorectal cancer through PTEN-Mediated PI3K/AKT pathway. Ann Surg Oncol 22: 2649-2655, 2015.
29. Cooper J and Giancotti FG: Molecular insights into *NF2*/Merlin tumor suppressor function. FEBS Lett 588: 2743-2752, 2014.
30. Rong R, Tang X, Gutmann DH and Ye K: Neurofibromatosis 2 (NF2) tumor suppressor merlin inhibits phosphatidylinositol 3-kinase through binding to PIKE-L. Proc Natl Acad Sci USA 101: 18200-18205, 2004.